18TH WORLD CONFERENCE ON EARTHQUAKE ENGINEERING
WCEE2024
MILAN

MILAN, ITALY
30TH JUNE - 5TH JULY 2024

www.wcee2024.it

SEISMIC RESPONSE COMPARISON OF A HISTORICAL MASONRY CHURCH SUBJECT TO REAL AND SIMULATED GROUND MOTIONS

S. M. Sajad Hussaini[1], Claudio Sebastiani[2], Monica Capasso[2], Valerio Sabbatini[2], Shaghayegh Karimzadeh[1], Sanaz Rezaeian[3], Silvia Santini[2], Paulo B. Lourenço[1]

[1]Department of Civil Engineering, Institute for Sustainability and Innovation in Structural Engineering, (ISISE), ARISE, University of Minho, Guimarães, Portugal.

[2]Department of Architecture, Roma Tre University, Rome, Italy.

[3]U.S. Geological Survey, Golden, CO, USA.

Corresponding author's email: valerio.sabbatini@uniroma3.it

Abstract: *In recent years, advanced numerical models and high-performance computing have facilitated the utilization of ground motion time series in the assessment of the non-linear dynamic behavior of historic masonry structures. Since recorded accelerograms can be sparse for specific analysis conditions, stochastic ground motion simulations have become a viable alternative to overcome this limitation. This study simulates the recorded acceleration time series of the Central Italy 2016 earthquake event at the closest station to the town of Macerata using a site-based stochastic approach. The simulated motions are seismologically evaluated using a goodness-of-fit method in terms of various intensity measures. The simulated records, in conjunction with real records, are used to study the non-linear dynamic behavior of San Filippo Neri church located in Macerata. The church of San Filippo represents an important example of Baroque religious architecture in central Italy, which was damaged and closed off to the public after the 2016 earthquake events. The construction was investigated with a vast diagnostic campaign which included on-site testing and dynamic identification tests. The collected data is used to calibrate the dynamic response of a three-dimensional finite element model of the church. The model is finally used to compare the non-linear seismic responses under real and simulated ground motions with the site recorded damage. The results of structural responses demonstrate a strong agreement between the real and simulated records, providing evidence to support the validation of the site-based stochastic simulation.*

1. Introduction

The preservation of historical masonry structures in seismic-prone regions presents a multifaceted challenge. These important architectural heritages, often rich in history and artistic significance, are not only testament to the past but also active components of our contemporary built environment. Therefore, ensuring their resilience against seismic events is not merely an engineering endeavor but a commitment to safeguarding our cultural legacy.

Traditionally, the seismic assessment of historical masonry buildings involves subjecting the structure to recorded ground motions from past earthquakes to perform structural evaluations. However, the challenges arise when there is a scarcity of recorded strong ground motions for the region or scenario of interest. In such

cases, engineers often resort to using artificial or synthetic ground motions. Artificial ground motions are generated by selecting and modifying recorded time series. However, these methods can be contentious because they have the potential to yield ground motion time series that are unrealistic, primarily due to their altered correlation with the real earthquake scenario (Naeim and Lew, 1995; Luco and Bazzurro, 2007). Synthetic ground motions are generated by employing a ground motion simulation model. These models can be categorized into deterministic source-based (also known as physics-based), stochastic source-based and stochastic site-based, and hybrid approaches (Graves and Pitarka, 2010; Rezaeian and Sun, 2014; Moratto, Vuan and Saraò, 2015). The widespread use of sophisticated deterministic source-based approaches in general engineering practice is often prevented by their high computational expenses and in-depth seismological knowledge of ground media (Douglas and Aochi, 2008; Rezaeian and Sun, 2014). Similarly, the stochastic source-based approach relies on parameters that can exhibit substantial variations across different regions where seismological studies may be unavailable (Chouet, Aki and Tsujiura, 1978). This limits its applicability within the general engineering practice. The stochastic site-based methods are often more appealing to engineering practice since they offer less computational cost with fewer input parameters (Rezaeian and Der Kiureghian, 2008; Stafford, Sgobba and Marano, 2009; Rezaeian and Sun, 2014). The main goal of stochastic site-based methods is to replicate the important characteristics of a real ground motion time series using an underlying stochastic process. The synthetic ground motions and the simulation model should be validated before any use in engineering practice. A comprehensive review of the literature uncovers studies where simulations have been validated in specific cases within both seismological and engineering contexts (Ugurhan *et al.*, 2012; Rezaeian *et al.*, 2015; Can, Askan and Karimzadeh, 2021; Ozsarac *et al.*, 2021). However, there is limited utilization of simulated motion in the literature when it comes to historical masonry buildings (Hoveidae, Fathi and Karimzadeh, 2021; Karimzadeh *et al.*, 2023).

The building selected for this study is the historic masonry church of San Filippo Neri, located in the historical center of Macerata, Italy. This building is particularly interesting due to the clear evidence of structural damage caused by the Central Italy 2016 earthquake, which led to its closure to the public. In 2018, an extensive testing and monitoring campaign was conducted to identify the main material and modal parameters of the church. The combination of visible damage and experimental values supported the development of a finite element model (FEM) for conducting a series of nonlinear dynamic analyses.

This paper investigates the seismic response of San Filippo Neri church. A set of synthetic ground motion time series is generated using a stochastic site-based approach (Rezaeian and Der Kiureghian, 2008). The investigation compares the church's performance under real recorded ground motion against that under synthetics replicating the same seismic scenario. Through this comparative study, we aim to shed light on the validity of the stochastic simulation method while gaining deeper insights into the structural behavior of the church.

2. Ground motion simulation

This section provides details about the ground motion simulation method, including the identification of parameters calibrated for simulating the Central Italy 2016 earthquake.

2.1. Site-based stochastic approach

This study employs the fully non-stationary stochastic site-based model proposed by Rezaeian and Der Kiureghian (2008). This model describes a ground motion at a specific site by modulating a filtered white noise process. The form of the model is expressed as:

$$x(t) = q(t,\alpha)\left\{\frac{1}{\sigma_h(t)}\int_{-\infty}^{t} h\big(t-\tau,\lambda(\tau)\big)w(\tau)d\tau\right\} \quad (1)$$

where $x(t)$ is the acceleration time series, $q(t,\alpha)$ is a deterministic time modulating function that shapes the temporal evolution, $h(t-\tau,\lambda(\tau))$ is the impulse response function of the filter, $w(\tau)$ is the white-noise process, and $\sigma_h(t)$ is the standard deviation of the integral process.

To account for temporal non-stationarity, a gamma modulating function is used as expressed below:

$$q(t,\alpha) = \alpha_0 t^{\alpha_1} e^{-\alpha_2 t} \quad (2)$$

where $\alpha_0, \alpha_1, \alpha_2$ are the shape parameters of the function. In accordance with Rezaeian and Der Kiureghian (2008), the pseudo acceleration response of a single-degree-of-freedom linear oscillator is selected for the filter function, which contains time-varying parameters. The filter function is given as:

$$h\big(t-\tau,\lambda(\tau)\big) = \frac{\omega(\tau)}{\sqrt{1-\zeta^2(\tau)}} e^{-\zeta(\tau)\omega(\tau)(t-\tau)} \sin\left(\omega(\tau)\sqrt{1-\zeta^2(\tau)}(t-\tau)\right) \quad 3$$

where ω and ζ are the natural frequency and damping ratio of the filter. A linear function for the natural frequency and an exponential function for the damping ratio are considered to account for their time variations as expressed below:

$$\omega(t) = \omega_0 - \frac{\omega_0 - \omega_n}{t_n} t \quad 4$$

$$\zeta(t) = \zeta_0 e^{\ln\left(\frac{\zeta_0}{\zeta_1}\right)\frac{t}{t_n}} \quad 5$$

where ω_0 and ζ_0 are the frequency and damping ratio at the start time $t = 0$, and ω_n and ζ_n are the same at the end of duration $t = t_n$. Following Rezaeian and Der Kiureghian (2008), a critically damped second-order oscillator for high-pass filtering the process in Equation (1) is employed. This step is required to correct the long period spectral accelerations and to remove the residual values in the velocity and displacement time series. The corrected acceleration record, denoted by $\ddot{z}(t)$, is obtained from the solution of the differential equation as given below:

$$\ddot{z}(t) + 2\omega_c \dot{z}(t) + \omega_c^2 z(t) = x(t) \quad 6$$

Following Rezaeian and Der Kiureghian (2012), the described simulation model and corresponding parameters can be employed for the simulation of two orthogonal horizontal components of ground motion time series. Two orthogonal horizontal components of a target ground motion can be rotated to their so-called principal axes where the correlation coefficient between the two components becomes zero (Penzien and Watabe, 1974). Therefore, an independent stochastic model can be employed to simulate each rotated component.

2.2. Parameter identification for the target accelerogram

In this study, the orthogonal horizontal components of ground motion time series recorded at the Macerata station during the Central Italy 2016 earthquake ($M_w = 6$) is considered (Luzi *et al.*, 2016) (https://esm-db.eu). Following the procedure in Rezaeian and Der Kiureghian (2012), the recorded ground motion components are rotated to their principal axes with the rotation angle determined to be $\theta = 64.62°$. Therefore, two independent stochastic models are considered, corresponding to two components of the target motion.

To identify the parameters of each model, the statistical properties of the stochastic process described in Equation (1), including evolving intensity and frequency contents, are fitted to those of the corresponding component of the recorded ground motion in accordance with the objective functions reported in Rezaeian and Der Kiureghian (2008). This involves matching the cumulative expected energy of the stochastic process with that of the recorded ground motion component, which yields the three parameters of the gamma modulating function. Similarly, the cumulative expected number of zero-level up-crossings of the stochastic process and the average cumulative number of positive minima and negative maxima of ten simulated processes are fitted to those of the recorded ground motion component, resulting in the identification of the four parameters of the filter function. However, since high pass filtering in the model described in Equation (1) is conducted after parameter identification and generating time series, the objective function reported in Rezaeian and Der Kiureghian (2008) may not be satisfied anymore. It means that additional post processing results in a lower count of zero-level up-crossing and particularly positive-minima and negative-maxima. To address this issue, the corresponding objective functions in Rezaeian and Der Kiureghian (2008) are optimized again for each component of ground motion after considering an appropriate corner frequency for the high pass filter in a trial-and-error procedure. The high pass filter is conducted using $\omega_c = 0.25\ Hz$ on both components. Table 1 shows the identified parameters of the models corresponding to each rotated direction.

Table 1 Identified model parameters.

Rotated Component	Modulating parameters			Frequency parameters (Hz)		Damping ratio parameters	
	α_0	α_1	α_2	ω_0	ω_n	ζ_0	ζ_n
East-West	29.8	0.23	0.12	2.95	1.2	0.5	0.1
North-South	4.8	1.9	0.3	4.2	0.7	0.9	0.1

3. Numerical modeling

3.1. Masonry prototype

The church of San Filippo Neri in Macerata represents an extraordinary example of Italian Baroque architecture. The construction was completed in 1732 under the guidance of Sebastiano Cipriani, following the design of the famous Architect Giovan Battista Contini (Ricci, 1834). The church is formed by a rectangular narthex, the main oval aula is surrounded by four radial chapels and covered by an elliptical dome with a lantern (Figure. 1a). In 2016, a series of seismic events affected Macerata, causing damage to the church. The main structural damage consisted of a series of cracks along the dome in the longitudinal direction (Figure. 1c) and crossing the drum above the apse (Figure. 1b) and vestibule (Figure. 1d), moreover minor cracks were reported on the lantern (Figure. 1e).

(a) (b) (c) (d) (e)

Figure. 1 (a) The church of San Filippo Neri, view from the main façade (West side), (b) cracks crossing the drum above the apse and along the dome (East side), (c) cracks on the dome along the longitudinal direction (East-West direction), (d) cracks across the drum above the vestibule and along the dome (West side), (e) cracks on the top lantern.

In July 2018, Prisma Laboratory of the Architecture Department of Roma Tre University carried out an extensive testing and monitoring campaign on the church (Santini *et al.*, 2021). The most relevant experimental results for the purpose of this research are the four double flat jack tests. In these tests, expandable rubber membranes, known as flat jacks, were employed to measure in-situ stress and deformation characteristics. These tests were conducted on the external north and south lateral walls, the south-east pillar, and the boundary wall between the church and the adjacent building. Additionally, ambient vibration tests (AVT) were performed as reported in Table 2.

Table 2 Experimental results of the diagnostic campaign (Santini et al.*, 2021).*

Double Flat Jack test				Ambient Vibration Test			
Test location	E [MPa]	v	f_c [MPa]	Mode	f [Hz]	ξ [%]	Description
North Wall	3800	0.26	3.45	1	2.06	1.11	Translational in the transversal direction
South Wall	7400	0.30	3.35	2	2.97	2.84	Translational in the longitudinal direction
South-east Wall	2900	-	3.01	3	3.39	1.45	Rotational
Boundary Wall	1546	0.30	2.56	4	4.17	1.27	Rotational of the East portion

Following Santini et. al. (2021), a three-dimensional finite element model of the church was defined with 253,085 solid elements and 73,553 nodes assuming fixed-based conditions and lateral horizontal constraints for the building adjacent to the church (Figure. 2a). To reduce the computational burden of the analysis, the material nonlinearity is only considered for the historical masonry of the church (in blue) while the masonry of the adjacent building was assumed as linear elastic (in yellow). The numerical model was calibrated based on the experimental data (Baggio, Sabbatini and Santini, 2019). Young's modulus of the numerical model was decreased by 50% from the experimental values to reduce the overestimation of the parameter due to the test and to shift the numerical modal frequencies closer to the experimental, assuming a preexisting partially cracked condition of the materials. Moreover, the mass density was incremented from 18 to 20 kN/m^3 to account for the nonstructural elements disregarded in the numerical model. The dynamic behaviour of the FEM model has been numerically investigated through modal analysis. From the results, it appears that the first vibrational mode occurs at a frequency of 3,00 Hz with a participating translational mass of 47,91% in the Y direction. Similarly, the second vibrational mode occurs at a frequency of 4,61 Hz with a participating translational mass of 39,54% in the X direction. Instead, the third vibrational mode occurs at a frequency of 5,14 Hz with a participating rotational mass of 10,59% in the Z direction.

The solid brick masonry of the church, which is constructed using lime-based mortar, is modeled as a homogenized material following the Concrete Damage Plasticity formulation. This formulation describes the irreversible damage that occurs during the fracturing process of quasi-brittle materials like masonry under relatively low confining pressure. It considers the different stiffness reductions during unloading in tension or compression and incorporates the stiffness recovery effects during cyclic load reversals. The model accounts for the damage variable (D), which assumes a value equal to zero in the absence of damage (elastic domain), and equal to one in the case of total loss of strength. Figure. 2b. illustrates in blue, the stress-strain curves for pure tension (positive y-axis) and pure compression (negative y-axis). Additionally, on the same graph, the damage curve is superimposed in red, with the y-axis representing damage and the x-axis representing longitudinal strain.

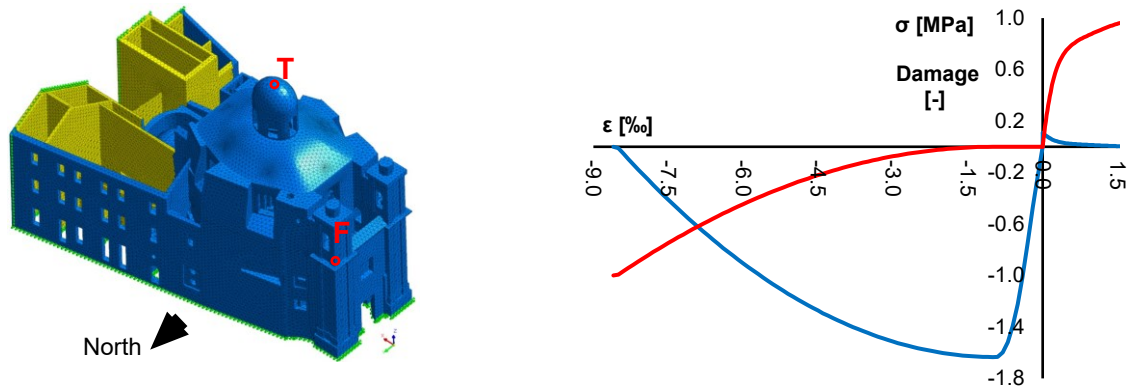

(a) (b)

Figure. 2 (a) Finite Element Model, (b) Stress-strain and damage-strain relationships for the masonry of the church of San Filippo Neri.

3.2. Comparison framework

Nonlinear time history analysis is considered to numerically simulate the seismic behavior of the church under orthogonal horizontal components of ground motion time series of 10 s each (time step of 0.01 s) and work convergence criteria (1% error tolerance).

The top node of the lantern (T) and the node at the base of the tower of the façade (F) were selected as control nodes for comparison of the horizontal displacements over time (Figure. 2a). Control point T is located in the top central part of the church on the symmetry axis at 35.7 m height, control point F is located on the north-west corner at 16.8 m height. The trajectories of these two control points are assumed representative of the overall structural response for each analysis. In addition, the cumulative damage is compared with the crack survey in terms of the location of the highest tension damage, aiming for the validation of the numerical results.

4. Result and Discussion

The following section provides information concerning the results of ground motion simulation and structural analysis.

4.1. Assessment of simulated ground motions

In this study, we assess the agreement between the observed and seven pairs of stochastically simulated data (referred to as Sim1 to Sim7) at the chosen station using a visual comparison including Fourier amplitude spectrum (FAS) and spectral acceleration (SA) as well as various goodness of fit (GOF) measures for each directional component as described in Olsen and Mayhew (2010). Figure. 3 and Figure. 4 illustrate the FAS and SA of the target and simulated motions, respectively. It is apparent that the target motion falls within the range covered by the simulated motions, providing a visually satisfactory assessment of the simulations.

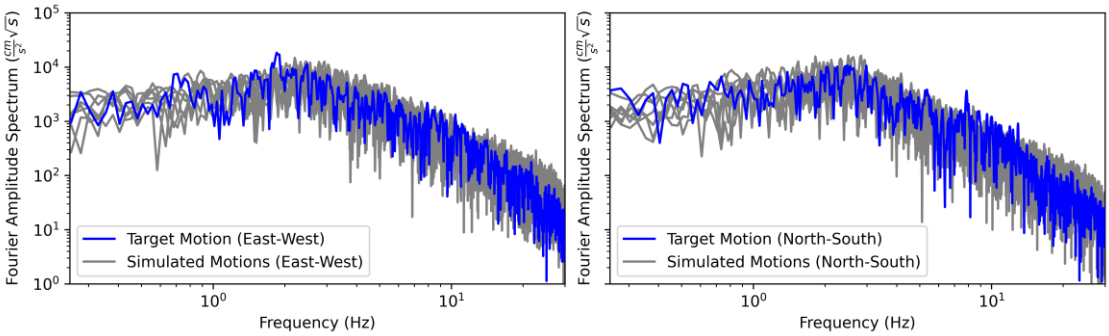

Figure. 3 Fourier amplitude spectrum for the target and simulated motions corresponding to each direction.

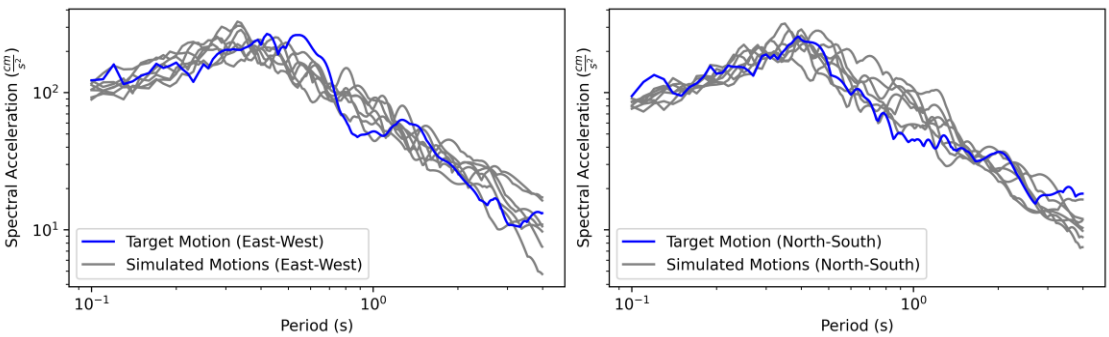

Figure. 4 Spectral acceleration for the target and simulated motions corresponding to each direction.

The GOF evaluation focuses on alternative intensity measures (IMs), including peak ground acceleration (PGA), peak ground velocity (PGV), the ratio of peak ground velocity to peak ground acceleration (PGV/PGA), Arias intensity (AI) (Arias, 1970), cumulative absolute velocity (CAV) (Reed and Kassawara, 1990), acceleration spectrum intensity (ASI) (von Thun et al., 1988), modified acceleration spectrum intensity (ASI) for the period range of 0.1 to 2.5 seconds, velocity spectrum intensity (VSI) (Yakut and Yılmaz, 2008), Housner intensity (HI) (Housner, 1959), bracketed duration (Dbr), Fourier amplitude spectrum (FAS*) within the frequency range of 0.25 to 10 Hz, and spectral acceleration (SA) within the period range of 0.1 to 4 seconds. Table 3 shows the qualitative classification of the GOF score according to Olsen and Mayhew (2010). However, it is important to recognize that these scores are subjective and can vary depending on the selected IMs (Karimzadeh et al., 2023). The reason is that different IMs may emphasize certain aspects of the observed and simulated data differently. Each IM has its own unique way of quantifying ground motion characteristics, such as amplitude, frequency content, and duration. Consequently, the choice of IMs can significantly impact the assessment of GOF because it highlights specific aspects of the seismic response (Karimzadeh et al., 2023). The GOF scores in terms of considered IMs and their mean score are shown in*
Table 4. Typically, the majority of simulations fall into the "excellent fit" category. This outcome aligns with expectations, as the stochastic approach employs a fitting procedure intended to replicate the important characteristics of the recorded motions. Most IMs demonstrate an excellent or very good fit, except for FAS*, where the fit is classified as “poor”. This discrepancy primarily arises from two key factors. Firstly, the stochastic

model attempts to capture the time-varying frequency content of the target motion by relying on time-domain zero-crossing characteristics, which may offer only a rudimentary representation of the frequency content. Secondly, the model employs a filter function that yields only a single evolutionary pre-dominant frequency, contributing to the observed poor fit in the case of FAS*. Overall, the results suggest that the set of simulated ground motions is seismologically acceptable.

Table 3 GOF score classification (Olsen and Mayhew, 2010).

Category	Excellent fit	Very good fit	Fair fit	Poor fit	Bad fit
GOF score range	80-100	65-80	45-65	35-45	<35

Table 4 GOF scores for considered intensity measures of the simulated set.

Component		PGA	PGV	PGV/ PGA	AI	CAV	ASI	ASI*	VSI	HI	Dbr	SA	FAS*	Mean
Sim 1	EW	88	88	100	76	74	97	94	97	96	49	74	44	81
	NS	85	76	90	97	85	93	85	85	87	70	73	43	81
Sim 2	EW	92	93	85	84	77	96	100	82	92	46	67	47	80
	NS	83	69	85	89	94	97	91	83	91	76	77	42	81
Sim 3	EW	96	91	94	75	75	95	96	78	83	59	68	44	80
	NS	81	95	77	96	93	93	93	88	88	71	74	42	83
Sim 4	EW	82	77	95	72	73	91	94	97	99	46	76	46	79
	NS	92	71	78	75	99	91	88	88	97	77	72	41	81
Sim 5	EW	87	79	92	85	83	87	96	93	98	56	77	43	81
	NS	97	90	93	95	92	91	91	85	92	72	62	44	84
Sim 6	EW	76	88	88	88	77	93	92	95	92	50	63	45	79
	NS	89	93	96	90	89	83	92	89	92	76	70	44	84
Sim 7	EW	91	92	98	81	80	99	93	99	100	53	61	47	83
	NS	94	99	92	92	89	98	73	68	73	62	67	41	79

4.2. Structural analysis results

Figure. 5 illustrates the horizontal displacements of control nodes F and T for each analysis. The results indicate that the displacements in the transversal direction (y) are two to four times greater than those in the longitudinal direction (x). These displacements present the directional structural response of the prototype. The largest displacements which correspond to Sim2, Sim3, and Sim4 (Figure. 5c, d, e) show asymmetrical responses. Conversely, the smallest displacements are associated with Sim1, Sim5, and Sim7, all of which display symmetrical responses.

Nodal displacements are subjected to second-order polynomial regression to capture directional variations. The coefficient of determination (R^2) values for real ground motions are the highest, with 63% at node F and 32% at node T. Sim3 follows as the second highest, with 46% at node F and 12% at node T, while Sim7 exhibits the lowest values, with 10% at node F and 1% at node T. Consequently, the simulated ground motions demonstrate greater variability in their trajectories compared to real ground motion responses.

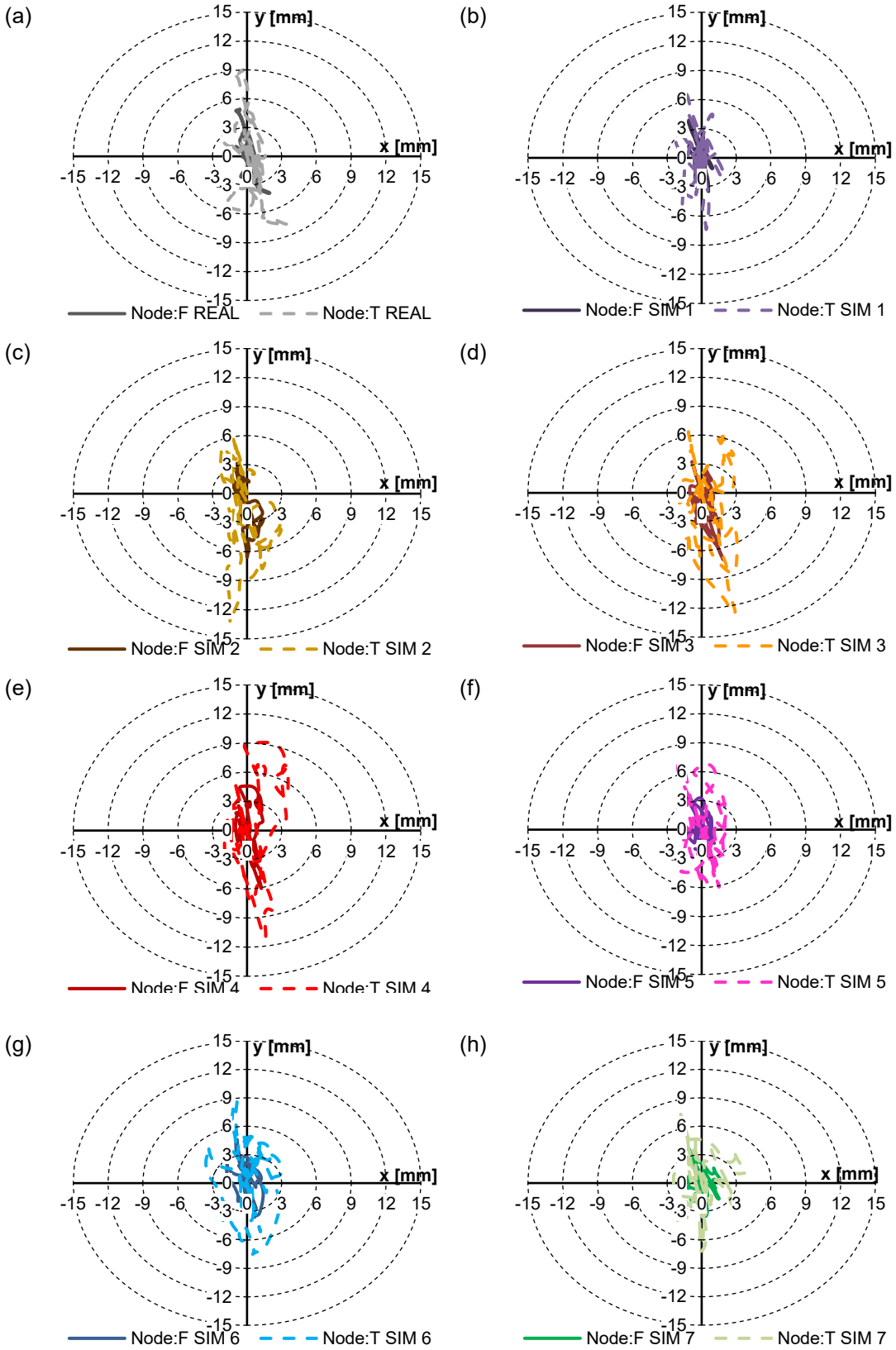

Figure. 5 Displacement responses of control node F and T from (a) real recorded, (b) Sim1, (c) Sim2, (d) Sim3, (e) Sim4, (f) Sim5, (g) Sim6, (h) Sim7 simulated ground motions.

The displacement responses are ordered from largest to smallest to assess the variation in terms of intensities. The horizontal displacements at nodes F and T are divided into five distinct ranges: 0 to 3 mm, 3 to 6 mm, 6 to 9 mm, 9 to 12 mm, and 12 to 15 mm as shown in Figure. 6. Sim3 exhibits the highest displacements,

followed by Sim2, Sim4, Real, Sim6, Sim5, Sim1, and Sim7, in descending order. Consequently, the absolute value of the response displacement from the real ground motion contributes to the average of the responses from the simulated ground motions.

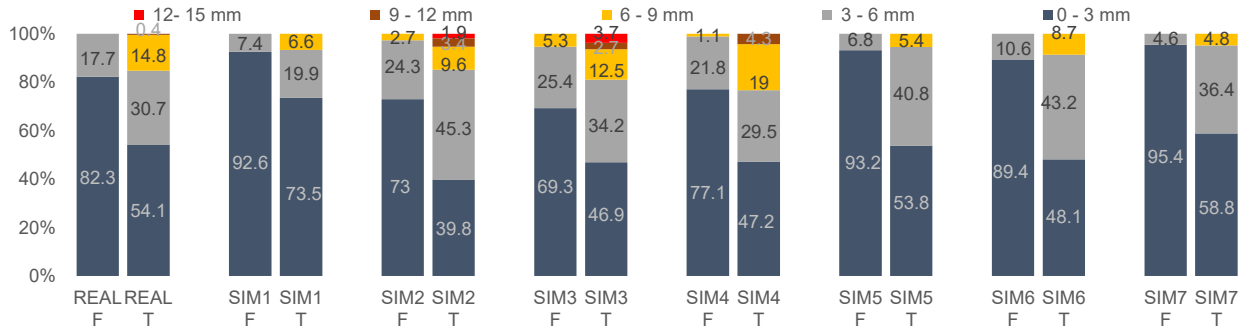

Figure. 6 Displacement responses of nodes F and T, subdivided into five intensity ranks.

The magnitude of response displacement is directly correlated with the extent of damage (Karimzadeh *et al.*, 2023). In Figure. 7, the cumulative tension damage and the percentage of material exceeding 30% damage, are presented. Among these scenarios, Sim3 (Figure. 7d) exhibits the most severe scenario, with 15.1% of material experiencing significant damage (corresponding to the largest displacement). In contrast, for the real ground motion (Figure. 7a), this value is 8.9%, falling within the range of average damage. Notably, the most extensive damage is observed in the following order: Sim3, Sim4, and Sim2 (as shown in Figure. 7d-e), aligning with the largest asymmetrical displacements. The damage distribution is consistent in all the analyses which fairly replicate the cracks crossing the drum above the apse and along the east portion of the dome.

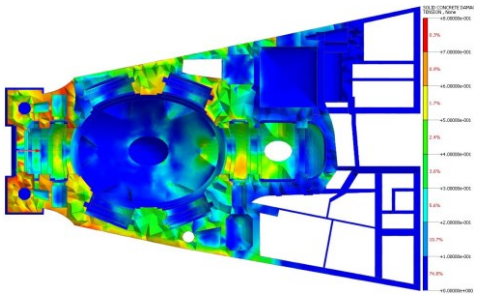

(a) 8.9 % > 0.3 D

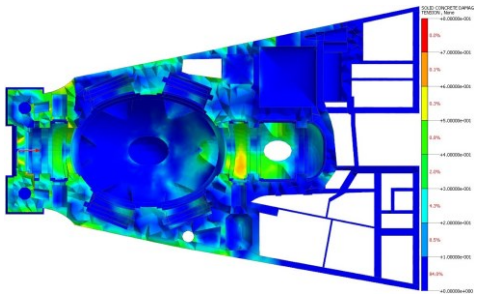

(b) 3.2 % > 0.3 D

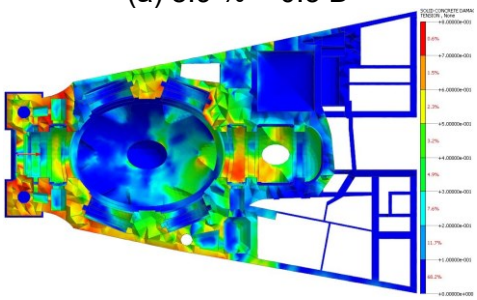

(c) 12.5 % > 0.3 D

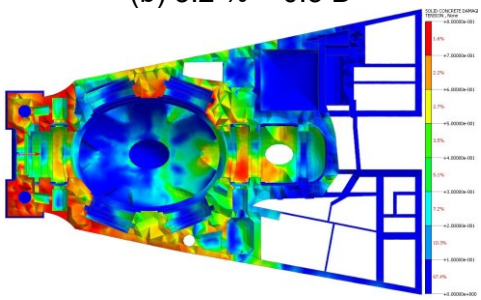

(d) 15.1 % > 0.3 D

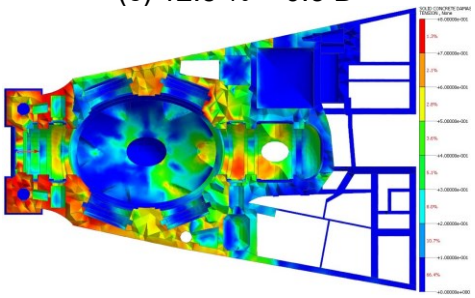

(e) 14.9 % > 0.3 D

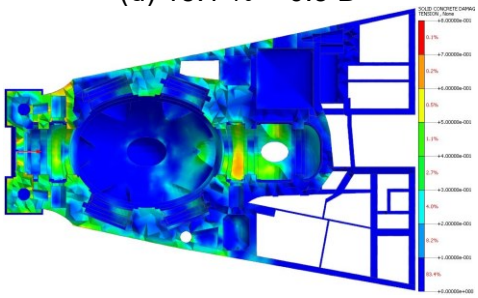

(f) 4.6 % > 0.3 D

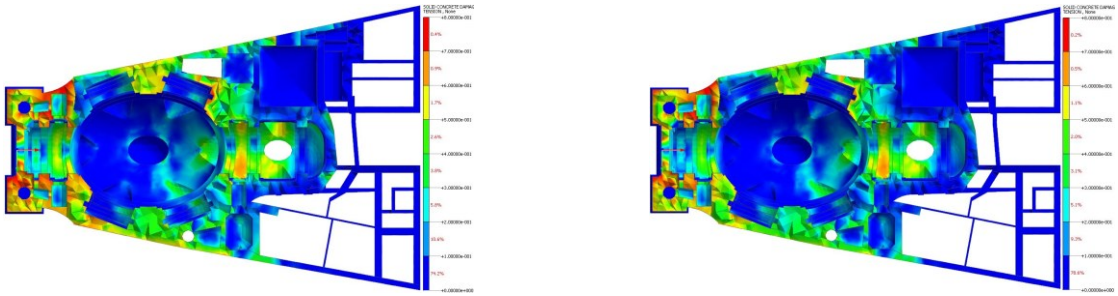

(g) 9.4 % > 0.3 D (h) 6.9 % > 0.3 D

Figure. 7 Bottom view of the cumulated tension damage at 10 sec for (a) real recorded, (b) Sim1, (c) Sim2, (d) Sim3, (e) Sim4, (f) Sim5, (g) Sim6, (h) Sim7 ground motions.

5. Conclusions

This study employs a site-based stochastic model to simulate the recorded ground motion during the Central Italy 2016 earthquake event at the Macerata station. Seven pairs of orthogonal horizontal simulated motions along with the recorded ones are used to investigate the seismic response of San Filippo Neri church located in Macerata, Italy. The nonlinear time history analyses of an experimentally calibrated model reveal a higher degree of spatial variability (within the structure) of the displacement responses for the simulated ground motions compared to those for the real ground motion. The magnitude of the displacement response from the real ground motion contributes to the average of the responses from the simulated ground motions. The consistent damage distribution across all analyses effectively reproduces the primary cracks observed in the church. Notably, the most extensive damage results from the simulated ground motions, corresponding to the largest asymmetrical displacement responses. These findings confirm the validation of simulated ground motions, establishing their suitability for design and assessment purposes. In particular, the stochastic model with identified parameters for the specific earthquake scenario can be employed to conduct a parametric study aimed at identifying the most influential intensity measures that impact the response of the masonry structure.

Acknowledgements

This work was partly financed by FCT/MCTES through national funds (PIDDAC) under the R&D Unit ISISE under reference UIDB/04029/2020, and under the Associate Laboratory Advanced Production and Intelligent Systems ARISE under reference LA/P/0112/2020. This work was partly financed by the STAND4HERITAGE project that has received funding from the European Research Council (ERC) under the European Union's Horizon 2020 research and innovation program (Grant agreement No. 833123), as an Advanced Grant. This work was partly financed by national funds through FCT - Foundation for Science and Technology, under grant agreement UI/BD/153379/2022 attributed to the first author.

Disclaimer

Any use of trade, firm, or product names is for descriptive purposes only and does not imply endorsement by the U.S. Government.

References

Arias, A. (1970) ‘A measure of earthquake intensity’, in *Seismic Design for Nuclear Power Plants*.

Baggio, C., Sabbatini, V. and Santini, S. (2019) ‘Model updating of a masonry historical church based on Operational Modal Analysis: the case study of San Filippo Neri in Macerata’, in. 10.7712/120119.7186.18559, pp. 3777–3792. Available at: files/618/Baggio et al. - 2019 - Model updating of a masonry historical church base.pdf.

Can, G., Askan, A. and Karimzadeh, S. (2021) ‘An assessment of the 3 February 2002 Cay (Turkey) earthquake (Mw=6.6): Modeling of ground motions and felt intensity distribution’, *Soil Dynamics and Earthquake Engineering*, 150, p. 106832. Available at: https://doi.org/10.1016/J.SOILDYN.2021.106832.

Chouet, B., Aki, K. and Tsujiura, M. (1978) ‘Regional variation of the scaling law of earthquake source spectra’, *Bulletin of the Seismological Society of America*, 68(1), pp. 49–79. Available at: https://doi.org/10.1785/BSSA0680010049.

Douglas, J. and Aochi, H. (2008) 'A Survey of Techniques for Predicting Earthquake Ground Motions for Engineering Purposes', *Surveys in Geophysics*, 29(3), pp. 187–220. Available at: https://doi.org/10.1007/s10712-008-9046-y.

Graves, R.W. and Pitarka, A. (2010) 'Broadband ground-motion simulation using a hybrid approach', *Bulletin of the Seismological Society of America*, 100(5 A), pp. 2095–2123. Available at: https://doi.org/10.1785/0120100057.

Housner, G.W. (1959) 'Behavior of Structures During Earthquakes', *Journal of the Engineering Mechanics Division*, 85(4). Available at: https://doi.org/10.1061/jmcea3.0000102.

Hoveidae, N., Fathi, A. and Karimzadeh, S. (2021) 'Seismic damage assessment of a historic masonry building under simulated scenario earthquakes: A case study for Arge-Tabriz', *Soil Dynamics and Earthquake Engineering*, 147, p. 106732. Available at: https://doi.org/10.1016/J.SOILDYN.2021.106732.

Karimzadeh, S. *et al.* (2023) 'Stochastic simulation of earthquake ground motions for the seismic assessment of monumental masonry structures: Source-based vs site-based approaches', *Earthquake Engineering & Structural Dynamics* [Preprint]. Available at: https://doi.org/10.1002/EQE.4012.

Luco, N. and Bazzurro, P. (2007) 'Does amplitude scaling of ground motion records result in biased nonlinear structural drift responses?', *Earthquake Engineering & Structural Dynamics*, 36(13), pp. 1813–1835. Available at: https://doi.org/10.1002/eqe.695.

Luzi, L. *et al.* (2016) 'The Engineering Strong-Motion Database: A Platform to Access Pan-European Accelerometric Data', *Seismological Research Letters*, 87(4), pp. 987–997. Available at: https://doi.org/10.1785/0220150278.

Moratto, L., Vuan, A. and Saraò, A. (2015) 'A Hybrid Approach for Broadband Simulations of Strong Ground Motion: The Case of the 2008 Iwate–Miyagi Nairiku Earthquake', *Bulletin of the Seismological Society of America*, 105(5), pp. 2823–2829. Available at: https://doi.org/10.1785/0120150054.

Naeim, F. and Lew, M. (1995) 'On the Use of Design Spectrum Compatible Time Histories', *Earthquake Spectra*, 11(1), pp. 111–127. Available at: https://doi.org/10.1193/1.1585805.

Olsen, K.B. and Mayhew, J.E. (2010) 'Goodness-of-fit Criteria for Broadband Synthetic Seismograms, with Application to the 2008 Mw 5.4 Chino Hills, California, Earthquake', *Seismological Research Letters*, 81(5), pp. 715–723. Available at: https://doi.org/10.1785/gssrl.81.5.715.

Ozsarac, V. *et al.* (2021) 'Seismic demands of bare and base-isolated steel frames for real against simulated records of a past earthquake', *https://doi.org/10.1080/15732479.2021.1895227*, 18(9), pp. 1266–1281. Available at: https://doi.org/10.1080/15732479.2021.1895227.

Penzien, J. and Watabe, M. (1974) 'Characteristics of 3-dimensional earthquake ground motions', *Earthquake Engineering & Structural Dynamics*, 3(4), pp. 365–373. Available at: https://doi.org/10.1002/eqe.4290030407.

Reed, J.W. and Kassawara, R.P. (1990) 'A criterion for determining exceedance of the operating basis earthquake', *Nuclear Engineering and Design*, 123(2–3), pp. 387–396. Available at: https://doi.org/10.1016/0029-5493(90)90259-Z.

Rezaeian, S. *et al.* (2015) 'Validation of Simulated Earthquake Ground Motions Based on Evolution of Intensity and Frequency Content', *Bulletin of the Seismological Society of America*, 105(6), pp. 3036–3049. Available at: https://doi.org/10.1785/0120140210.

Rezaeian, S. and Der Kiureghian, A. (2008) 'A stochastic ground motion model with separable temporal and spectral nonstationarities', *Earthquake Engineering & Structural Dynamics*, 37(13), pp. 1565–1584. Available at: https://doi.org/10.1002/eqe.831.

Rezaeian, S. and Der Kiureghian, A. (2012) 'Simulation of orthogonal horizontal ground motion components for specified earthquake and site characteristics', *Earthquake Engineering & Structural Dynamics*, 41(2), pp. 335–353. Available at: https://doi.org/10.1002/eqe.1132.

Rezaeian, S. and Sun, X. (2014) 'Stochastic Ground Motion Simulation', in *Encyclopedia of Earthquake Engineering*. Berlin, Heidelberg: Springer Berlin Heidelberg, pp. 1–15. Available at: https://doi.org/10.1007/978-3-642-36197-5_239-1.

Ricci, A. (1834) *Memorie storiche delle arti e degli artisti della Marca di Ancona*. Tipografia di Alessandro Mancini, Con Approv.

Santini, S. *et al.* (2021) 'Onsite Testing for Nonlinear Analysis of an Earthquake Damaged Historical Church in Italy', *Applied Sciences*, 11(24). Available at: https://doi.org/10.3390/app112411755.

Stafford, P.J., Sgobba, S. and Marano, G.C. (2009) 'An energy-based envelope function for the stochastic simulation of earthquake accelerograms', *Soil Dynamics and Earthquake Engineering*, 29(7), pp. 1123–1133. Available at: https://doi.org/10.1016/j.soildyn.2009.01.003.

von Thun, J.L. *et al.* (1988) 'Earthquake ground motions for design and analysis of dams', in *Earthquake Engineering and Soil Dynamics II - Recent Advances in Ground-Motion Evaluation: Proceedings of the Specialty Conference*.

Ugurhan, B. *et al.* (2012) 'Strong-Ground-Motion Simulation of the 6 April 2009 L'Aquila, Italy, Earthquake', *Bulletin of the Seismological Society of America*, 102(4), pp. 1429–1445. Available at: https://doi.org/10.1785/0120110060.

Yakut, A. and Yılmaz, H. (2008) 'Correlation of Deformation Demands with Ground Motion Intensity', *Journal of Structural Engineering*, 134(12), pp. 1818–1828. Available at: https://doi.org/10.1061/(ASCE)0733-9445(2008)134:12(1818).